Journal of Materials Chemistry A

PAPER

View Article Online
View Journal | View Issue

Cite this: J. Mater. Chem. A, 2018, 6, 5661

A highly rigid and gas selective methanopentacene-based polymer of intrinsic microporosity derived from Tröger's base polymerization†

Rhodri Williams,[a] Luke. A. Burt,[a] Elisa Esposito,[b] Johannes C. Jansen, *[b] Elena Tocci,[b] Carmen Rizzuto,[b] Marek Lanč,[c] Mariolino Carta *[d] and Neil. B. McKeown *[a]

Polymers of intrinsic microporosity (PIMs) have been identified as potential next generation membrane materials for the separation of gas mixtures of industrial and environmental relevance. Based on the exceptionally rigid methanopentacene (MP) structural unit, a Polymer of Intrinsic Microporosity (PIM-MP-TB) was designed to demonstrate high selectivity for gas separations. PIM-MP-TB was prepared using a polymerisation reaction involving the formation of Tröger's base linking groups and demonstrated an apparent BET surface area of 743 m^2 g^{-1} as a powder. The microporosity of PIM-MP-TB was also characterized by chain packing simulations. PIM-MP-TB proved soluble in chlorinated solvents and was cast as a robust, free-standing film suitable for gas permeation measurements. Despite lower gas permeability as compared to previously reported PIMs, high selectivities for industrially relevant gas pairs were obtained, surpassing the 2008 Robeson upper bound for H_2/CH_4 and O_2/N_2, (*e.g.*, P_{O_2} = 999 Barrer; α_{O_2/N_2} = 5.0) and demonstrating a clear link between polymer rigidity and selectivity. Upon aging, the permeability data move parallel to the Robeson upper bounds with a decrease of permeability, compensated by a related increase in selectivity. Mixed gas permeation measurement for CO_2/CH_4 and CO_2/N_2 mixtures confirmed the excellent selectivity of PIM-MP-TB for potentially relevant separations such as biogas upgrading and CO_2 capture from flue gas. Importantly, unlike other high performing PIMs, PIM-MP-TB is prepared in four simple steps from a cheap starting material.

Received 16th January 2018
Accepted 27th February 2018

DOI: 10.1039/c8ta00509e

rsc.li/materials-a

1. Introduction

Since Polymers of Intrinsic Microporosity (PIMs) were first reported in 2004,[1] a range of potential applications have been identified including catalysis,[2–5] chiral separations,[6] and as the active material in sensors[7,8] or ionic diodes.[9,10] In particular, PIMs with the ability to form flexible, robust, self-standing films have potential as membrane materials for anionic transport,[11] the separation of gases, vapours[12] or for nanofiltration.[13,14] Their exceptional potential for gas separation[15,16] is based on the high free volume generated from the inability of their contorted polymer chains to pack efficiently, which provides high permeability, while the lack of conformational freedom and rigidity, due to their fused-ring structures, ensures good permselectivity. The design concept of PIMs has produced polymers whose gas permeability data have redefined the Robeson upper bounds,[17–20] which quantify the state-of-the-art trade-off between the desirable properties of permeability and selectivity. Hence, PIMs have potential for various industrial gas separation applications such as the recovery of hydrogen (*e.g.*, H_2/N_2), oxygen- or nitrogen-enrichment of air (O_2/N_2), biomethane and natural gas purification (CO_2/CH_4) and carbon capture (CO_2/N_2). Previously, we and others[21,22] have demonstrated the benefit of using bridged bicyclic units in place of the less rigid spirobisindane and benzodioxin structures of conventional PIMs (*e.g.* PIM-1).[23] For example, PIM-EA-TB (Fig. 1a),[23] which is composed of ethanoanthracene (EA) structural units linked by Tröger's base (TB *i.e.* methanodiazocene) demonstrates exceptional selectivity and subsequent work showed that the replacement of EA with triptycene to give PIM-Trip-TB[24] (Fig. 1b) or benzotriptycene to give PIM-BTrip-TB[25] (Fig. 1c) improves further both gas selectivity and permeability.

Evaluation of a range of potential structural building units for PIMs, assisted by molecular modeling, suggested two adjustments that could be made to the bridged bicyclic

[a]EaStCHEM, School of Chemistry, University of Edinburgh, Joseph Black Building, David Brewster Road, Edinburgh, Scotland EH93FJ, UK. E-mail: neil.mckeown@ed.ac.uk

[b]Institute on Membrane Technology, ITM-CNR, Via P. Bucci 17/C, 87036 Rende (CS), Italy. E-mail: johannescarolus.jansen@cnr.it

[c]Department of Physical Chemistry, University of Chemistry and Technology, Prague, Technická 5, 166 28 Prague 6, Czech Republic

[d]Department of Chemistry, College of Science, Swansea University, Grove Building, Singleton Park, Swansea, SA2 8PP, UK. E-mail: mariolino.carta@swansea.ac.uk

† Electronic supplementary information (ESI) available. See DOI: 10.1039/c8ta00509e

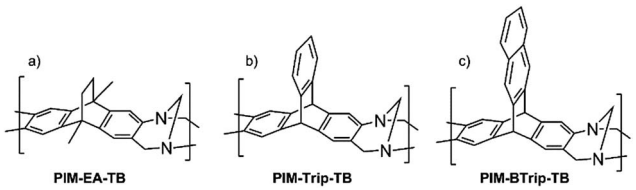

Fig. 1 PIMs based on TB linkages between (a) ethanoanthracene (b) triptycene or (c) benzotriptycene structural units.[23–25]

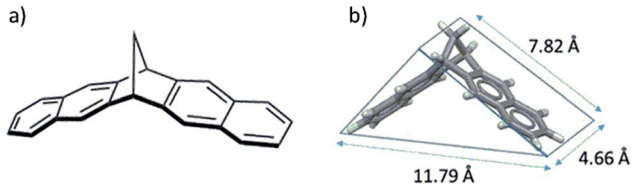

Fig. 2 (a) The structure of methanopentacene (MP); (b) XRD solid state crystal structure of MP.[27]

structural unit that might enhance further the rigidity of a TB-based PIM. Firstly, the use of a shorter methylene bridge and secondly, the incorporation of a greater proportion of aromatic rings within the polymer chain.[26] The readily prepared 6,13-dihydro-6,13-methanopentacene (MP)[27] hydrocarbon satisfied both of these design criteria (Fig. 2).[28]

2. Results and discussion

2.1. Polymer synthesis and characterization

Unsubstituted methanopentacene is easily prepared by the double Diels–Alder addition of the diene, dibromoquinodimethane, to norbornadiene (Scheme 1).[28] The required diene precursor to dinitromethanopentacene, 1,2-bis(dibromomethyl)-4-nitrobenzene (**2**), was synthesised by a convenient literature procedure in which a dilute solution of bromine is added slowly to the cheaply available 4-nitro-*o*-xylene (**1**) in chlorobenzene, whilst irradiating the reaction with a tungsten lamp.[29] This method avoids the use of highly toxic solvents such as carbon tetrachloride, and the high atom-inefficiency associated with brominating agents such as *N*-bromosuccinimide, reported in other procedures.[30,31] Treatment of **2** with sodium iodide eliminates bromine to produce the reactive intermediate dibromoquinodimethane, which combines with the commercial norbornadiene **3**, to give an isomeric mixture of 2,9(10)-dinitro-6,13-dihydro-6,13-methanopentacene (**4**) in 50% yield. This was reduced in the presence of hydrazine and RANEY® nickel, to obtain the required 2,9(10)-diamino-6,13-dihydro-6,13-methanopentacene monomer (**5**) as a mixture of isomers. The standard TB polymerisation procedure[23] was followed to afford PIM-MP-TB in 50% yield after purification by reprecipitation, which is similar to other TB-based PIMs.

It is well established that TB formation using 2-aminonaphthalene takes place exclusively at the 1-position of the naphthyl ring[32] so that the expected ideal structure of PIM-MP-TB is that shown in Scheme 1, albeit with no control over regiochemistry due to the mixture of two isomers of the monomer and the relative orientations of methylene bridges of the MP building unit and TB linking group (Fig. 3).

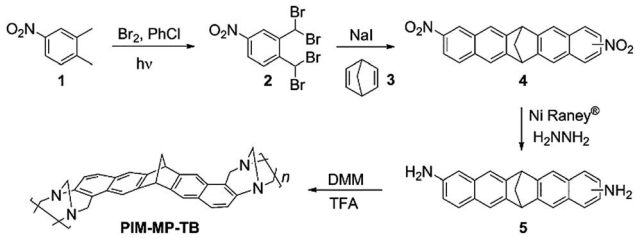

Scheme 1 Synthetic route to PIM-MP-TB (DMM = dimethoxymethane; TFA = trifluoroacetic acid).

Isothermal nitrogen adsorption confirmed the polymer to be significantly microporous with a BET surface area (SA_{BET}) of 743 $m^2 g^{-1}$. This is somewhat lower than the values obtained for PIM-EA-TB (1030 $m^2 g^{-1}$)[23] and other TB PIMs.[24–26,33] Thermogravimetric analysis (Fig. ESI3†) shows that the polymer is stable up to 400 °C (<3% loss), much higher than the EA–TB analogue, which undergoes a reverse Diels–Alder reaction[23] to release an ethylene fragment at around 260 °C.

2.2. Simulation of molecular structure and chain packing

To assess the relative flexibility of the PIM-MP-TB, the mechanical deformation of the MP structural unit was compared with that of triptycene,[24] ethanoanthracene[23] and TB. Fig. 4a shows the comparison of the energy cost as the dihedral angles in these units angle deviate from their most stable configuration, corresponding to the energy minimum as calculated using the Spartan 10.0 modelling package (Fig. 4b). The energy profiles for the framework distortion about dihedral angle 1 (Fig. 4a) are very similar for each structural unit (Fig. 4c). In contrast, those for dihedral angles 2 and 3 are sharper for MP than for the other units, confirming its greater rigidity (Table ESI1†). Simulation of chain packing for PIM-MP-TB was performed as described previously for PIM-EA-TB (ESI Section 6†) and optimized to a polymer density of 1.095 g cm^{-3} (Fig. 5a). This is only a small deviation from the experimental density of 1.13 g cm^{-3} for a freshly prepared film is 3.7% and hence is in reasonable agreement. The experimental density is higher than that reported for PIM-1 (1.092 g cm^{-3})[34] and of PIM-EA-TB (1.08 g cm^{-3}).[35] Free volume as determined by Bondi's

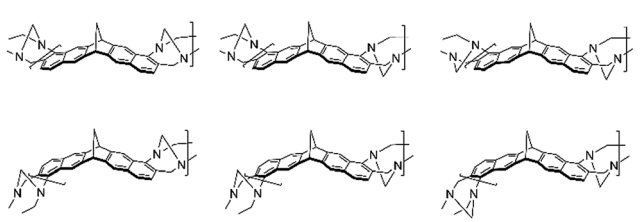

Fig. 3 The regiochemistry within the repeat unit of PIM-MP-TB due to the isomeric mixture of the monomer and the relative orientations of methylene bridges of the MP building unit and TB linking group.

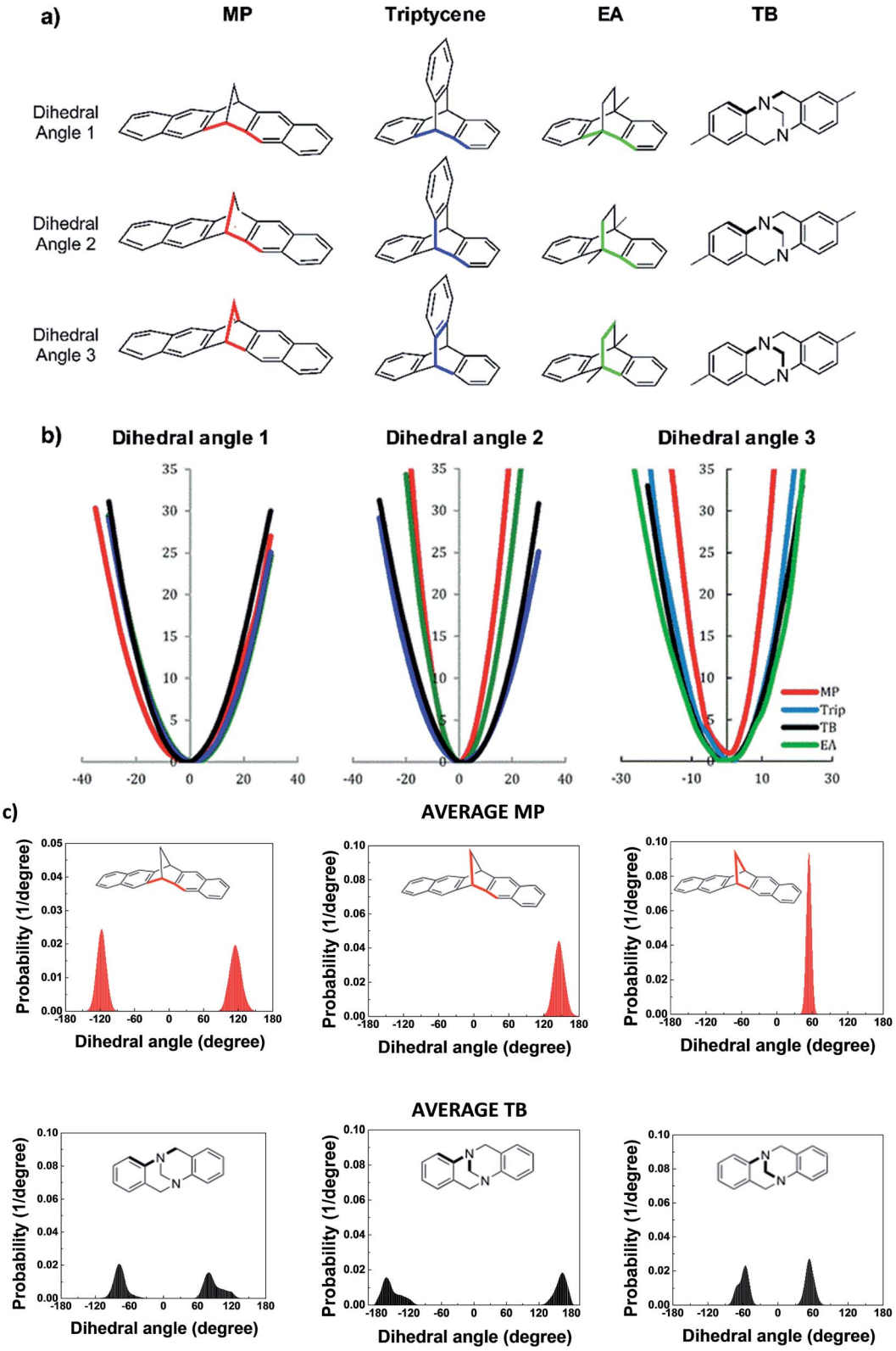

Fig. 4 (a) The defined dihedral angles in methanopentacene (MP), triptycene (Trip), ethanoanthracene (EA) and TB units; (b) potential energy surfaces of dihedral angles (DA) 1, 2 and 3 for MP, EA, triptycene and TB. (c) Dihedral angle distribution for the MP (red) and TB (black) units derived from packing simulations model.

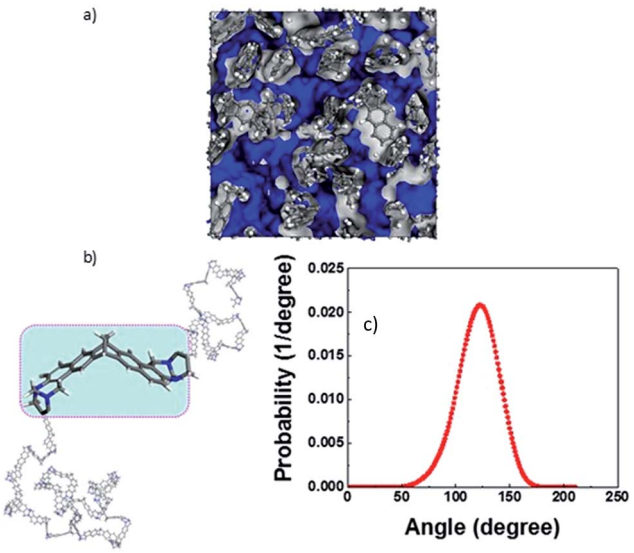

Fig. 5 (a) Molecular model of the polymer structure with a calculated density of 1.095 g cm^{-3}. The free volume elements are indicated as blue bubbly shapes. Length of the box edges is about 32 Å. (b, c) Structure and "bite" angle distribution of the MP unit in the optimized polymer chains.

method was calculated to be 25.8 ± 0.5% which is slightly smaller than that of PIM-EA-TB (27.6%)[35] and of PIM-1 (28.8%).[36] The calculated fractional free volume confirms the poor polymer packing that is typical for all PIMs. The dihedral angle distribution for the MP structural unit observed within the packing simulation correlate well with the energy potential of deformation calculated by molecular dynamics (Fig. 5). The "bite" angle of the MP units in the optimized chains of PIM-MP-TB (Fig. 5b), shows a very wide distribution (Fig. 5c). The average angle is close to the value found for the XRD solid state crystal structure in Fig. 2, but the wide distribution shows that many monomeric units are either stretched or squeezed into a configuration far from their thermodynamic equilibrium. Similar deformations of structural units within packing models of PIMs have been observed previously for PIM-EA-TB and PIM-1.[34,37,38]

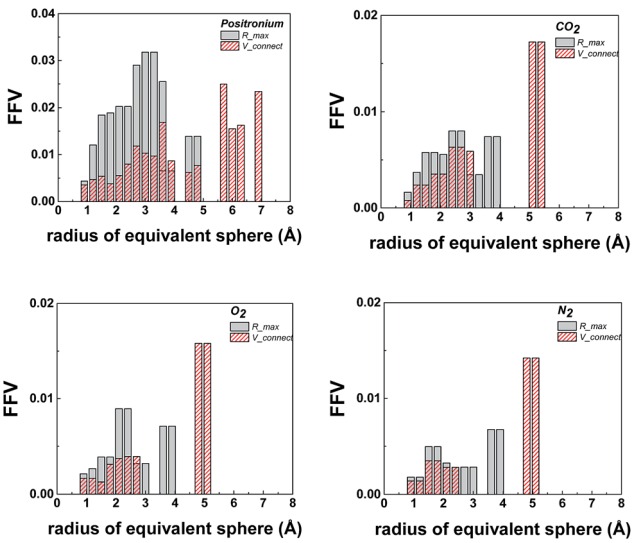

Fig. 6 Averaged size distribution functions using *O*-positronium (r = 1.1 Å), carbon dioxide (r = 1.65 Å), oxygen (r = 1.73 Å) and nitrogen (r = 1.82 Å) as probes using the Hofmann–Heuchel method.[39]

Fig. 5a shows a 3D representation of the free volume elements and their interconnectivity. Modelling of the pore size distribution by the method proposed by Hofmann and Heuchel[39] shows the presence of a majority of pores with an equivalent sphere radius in the range of 1–5 Å (*i.e.* pore diameter = 2–10 Å) (Fig. 6). The free volume element size distribution was quantified by the R_{max} and $V_{connect}$ approach, setting the probe diameter to the size of an *o*-positronium particle (r = 1.1 Å), carbon dioxide (r = 1.65 Å), oxygen (r = 1.73 Å) and nitrogen (r = 1.82 Å), and using a grid spacing of 0.5 Å. The maximum equivalent sphere radius in PIM-MP-TB is approximately 7 Å, which is smaller than for other other PIMs, such as PIM-1 (16.5–17 Å)[34] and PIM-EA-TB (15.5 Å).[35] This suggests that pores in PIM-MP-TB are both smaller and less interconnected relative to those in PIM-1 or PIM-EA-TB but similar to, for example, Hyflon®AD.[40]

The pore size distribution was calculated *via* NLDFT and H–K analysis of the CO_2 uptake at 273 K (Fig. ESI1†). Fig. 6 shows the pore size distribution of PIM-MP-TB. Qualitatively, PIM-MP-TB has a lower total pore volume and fewer pores over 5 Å, compared to PIM-EA-TB,[35] which correlates with its lower BET surface area and pore volume measured by gas adsorption.

2.3. Pure gas transport

Before permeability measurements, the films were soaked in methanol and dried to remove traces of residual casting solvent and to reverse the effect of physical aging.[37,38,41] The gas permeability, diffusivity and solubility coefficients, with the respective ideal selectivity, for the methanol-treated, aged and thermally treated films of PIM-MP-TB are given in Table 1. The precise sample history is given in Table ESI4.† The data are compared with those of the archetypal PIM-1 and PIM-EA-TB.

The order of permeability for the PIM-MP-TB is H_2 > CO_2 > He > O_2 > CH_4 > N_2, similar to that of PIM-EA-TB[12] but different to that of more permeable PIMs (PIM-Trip-TB and PIM-BTrip-TB),[24,25] in which CO_2 has a higher permeability than H_2, and O_2 has a higher permeability than He. This behavior indicates greater size selectivity for PIM-MP-TB as demonstrated by very high diffusivity selectivity (D_x/D_y) with respect to PIM-1, PIM-EA-TB and PIM-Trip-TB (Table 1). The high size selectivity is best seen from the very steep correlation between the diffusion coefficient and the effective diameter of the gas (Fig. 8). The excellent performance of PIM-MP-TB can be attributed to the superior rigidity of the MP bridged bicyclic unit, as discussed above. The high permselectivity, compared with that of many other PIMs, combined with moderately high permeabilities, places it close to the upper bound for the CO_2/CH_4 and CO_2/N_2 gas pair (Fig. 7a and c) and well above the 2008 upper bound for gas pairs involving H_2 (P_{H_2} = 4050 Barrer) with H_2/CH_4; α = 15.3 (Fig. 7b) and H_2/N_2 (α = 20.3). Furthermore, PIM-MP-TB

Table 1 Gas permeabilities P_x, diffusion coefficients D_x, solubility coefficients S_x, and ideal selectivities α (P_x/P_y), α (D_x/D_y) and α (S_x/S_y) at 25 °C for a methanol-treated film of PIM-MP-TB, PIM-EA-TB and PIM-1 with comparable thickness (94 μm, 95 μm and 93 μm, respectively) and for the aged and thermally treated samples of PIM-MP-TB

		Permeability, diffusivity and solubility						Selectivity α (P_x/P_y) α (D_x/D_y) α (S_x/S_y)				
Polymer (state[a])	Transport parameter	N_2	O_2	CO_2	CH_4	H_2	He	H_2/N_2	H_2/CH_4	CO_2/N_2	O_2/N_2	CO_2/CH_4
PIM-MP-TB (a)	P_x [Barrer]	200	999	3500	264	4050	1310	20.3	15.3	17.5	5.0	13.3
	D_x [10^{-12} m^2 s^{-1}]	18.3	106	26	6	2870	4640	157	478	1.42	5.8	4.33
	S_x [cm^3(STP) cm^{-3} bar^{-1}]	8.21	7.08	101	31	1.06	0.21	0.13	0.03	12.3	0.86	3.26
PIM-MP-TB (b)	P_x [Barrer]	125	648	2340	158	2790	956	22.3	17.7	18.7	5.18	14.8
PIM-MP-TB (c)	P_x [Barrer]	21.4	134	633	26	1120	492	52.3	43	29.6	6.26	24.4
PIM-MP-TB (d)	P_x [Barrer]	13.3	88.4	378	14.7	812	368	61	55.3	28.4	6.65	25.7
PIM-EA-TB (a)	P_x [Barrer]	380	1630	5100	572	7310	2720	19.2	12.8	13.4	4.29	8.92
	D_x [10^{-12} m^2 s^{-1}]	40.5	177	41	12	5000	6000	123	419	1.01	4.37	3.42
	S_x [cm^3(STP) cm^{-3} bar^{-1}]	7.04	6.91	93.3	35.75	1.10	0.34	0.16	0.03	13.2	0.98	2.61
PIM-1 (a)	P_x [Barrer]	773	2140	12 800	1280	4710	1830	6.1	3.68	16.6	2.77	10
	D_x [10^{-12} m^2 s^{-1}]	165	452	199	70	5760	7120	35	82	1.21	2.74	2.84
	S_x [cm^3(STP) cm^{-3} bar^{-1}]	3.52	3.54	48	13.7	0.61	0.19	0.17	0.04	13.6	1	3.5

[a] State: (a) methanol treated; (b) day 1 after thermal conditioning under vacuum at 140 °C; (c) after aging of 118 days and intermediate mixed gas permeation; (d) after 370 days of aging and intermediate mixed gas permeation. See ESI Table 4 for the complete sample history.

demonstrate a high oxygen permeability (P_{O_2} = 999 Barrer) showing higher O_2/N_2 selectivity (α = 5.0) with respect to PIM-EA-TB (α = 4.3), which is close to the revised 2015 upper bound[19] (Fig. 7d). The high O_2/N_2 selectivity confirms that the separation is strongly dependent on a molecular sieving mechanism, as O_2 has a smaller kinetic diameter (3.46 Å for O_2 and 3.64 Å for N_2) whereas both gases have a similar solubility in glassy polymers. Fig. 7 also demonstrates the effect of physical aging of PIM-MP-TB after different treatments. Upon ageing, the data points move almost parallel to the Robeson

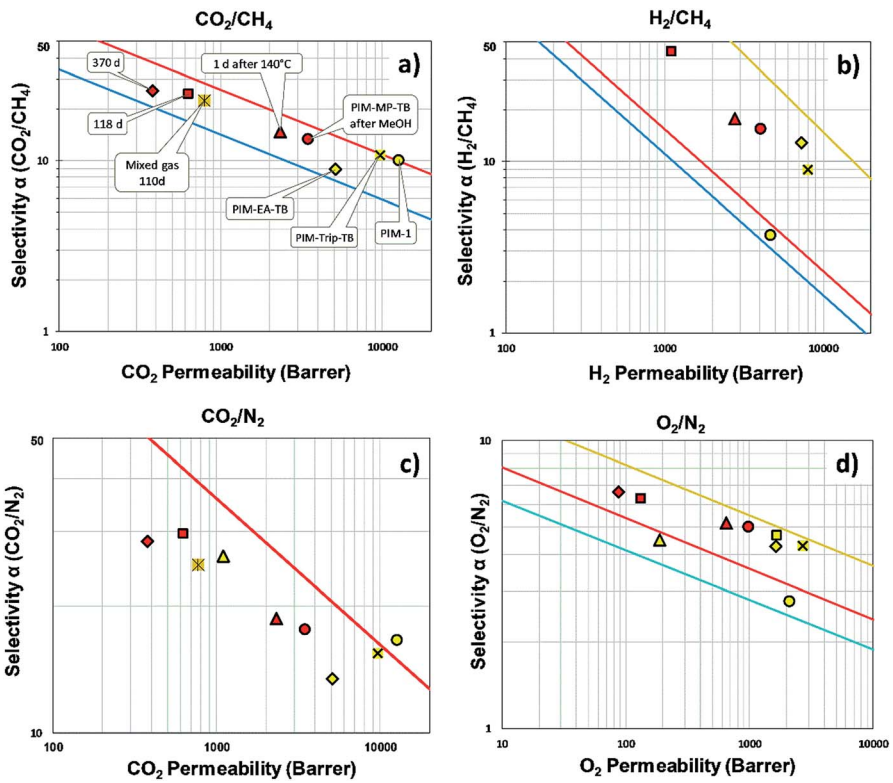

Fig. 7 Robeson plots of PIM-MP-TB for the CO_2/CH_4, H_2/CH_4, CO_2/N_2 and O_2/N_2 gas pairs after methanol treatment (●), aged for 1 (▲), 118 (■), 370 (◆) days after the thermal treatment at 140 °C under vacuum. Mixed gas data after 110 days aged (✱). The data for PIM-1 (●) and recent TB-PIMs like PIM-EA-TB (◆) and PIM-Trip-TB (✕) after MeOH are given for comparison. Feed pressure 1 bar and temperature 25 °C. The total aging time in days for each point is indicated as "*xxx* d".

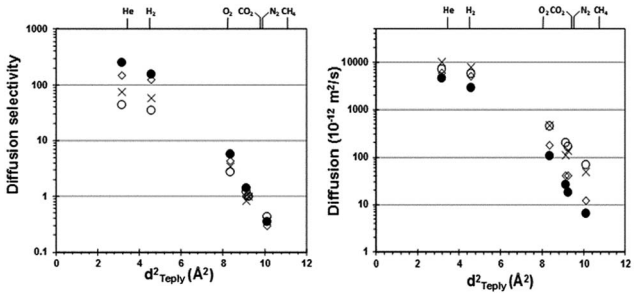

Fig. 8 Diffusion coefficients and corresponding selectivities *vs.* nitrogen as function of the squared effective diameter of the penetrant[42] gases for PIM-MP-TB (●), PIM-1 (○), PIM-EA-TB (◇) and PIM-Trip-TB (×).[25,35,37] Feed pressure 1 bar and temperature 25 °C.

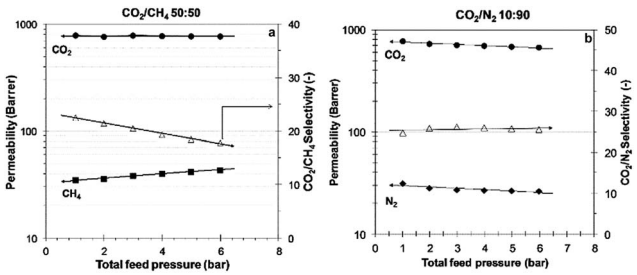

Fig. 9 (a) Pressure dependence of the CO_2 and CH_4 permeabilities with the corresponding CO_2/CH_4 selectivity, using the binary mixture CO_2/CH_4 (52.1 : 47.9 vol%); (b) pressure dependence of the CO_2 and N_2 permeabilities with the corresponding CO_2/N_2 selectivity, using the binary mixture CO_2/N_2 (10 : 90 vol%) 110 days aged PIM-MP-TB. Measurement temperature 25 °C.

upper bound, in the direction of higher selectivity and lower permeability compared to the methanol treated membrane. The thermal conditioning at 140 °C for 24 h just after methanol treatment (1 day aged), produces a similar effect suggesting that accelerated aging was achieved. After one year of ageing, with intermediate mixed gas permeation measurements, the performance remains still close to the 2008 Robeson upper bound for the CO_2/CH_4 and CO_2/N_2 separation, and above the upper bound for the H_2/CH_4, H_2/N_2 and O_2/N_2 gas pairs.

2.4. Mixed gas permeation

PIM-MP-TB also demonstrates promising permselectivity for mixed gas separation. Mixed gas permeability measurements were carried out using a sample aged for 110 days. Two different binary gas mixtures were used: CO_2/CH_4 (52.1/47.9 mol%) and CO_2/N_2 (10/90 mol%), simulating biogas with high CO_2 content and CO_2 poor flue gas, respectively. During the measurement, the pressure was increased stepwise from 1 to 6 bar (a) at 25 °C. Fig. 9 shows that for the CO_2/CH_4 mixture the CO_2 permeability is virtually independent from the pressure, whereas the CH_4 permeability slightly increases and, subsequently, the CO_2/CH_4 selectivity decreases with pressure. This suggests that the CO_2 induces matrix swelling, thus, facilitating CH_4 permeation. For the CO_2/N_2 mixture, both CO_2 and N_2 permeability slightly decrease as a function of the pressure and the selectivity remains nearly constant. Thus, PIM-MP-TB maintains excellent gas transport properties under mixed gas conditions for the CO_2/N_2 gas pair, close to the ideal selectivity ($\alpha = 29.6$).

3. Conclusions

The MP structural unit proved useful for making a high performing PIM. PIM-MP-TB demonstrated high selectivities for several important gas pairs such as O_2/N_2, H_2/N_2 and H_2/CH_4, well above the 2008 Robeson upper bounds and approach commercially useful separation factors for the aged film. The CO_2/N_2 ideal selectivity ($\alpha = 17.5$) is maintained under mixed gas conditions (10% CO_2 in N_2), up to 6 bar, which offers good potential for the application of PIM-MP-TB as a high flux first pass membrane in a two membrane system for CO_2 capture from flue gas. These results provide further evidence that molecular rigidity is a major determinant of intrinsic microporosity and high size selectivity. The molecular sieving performance, combined with the pore size distribution, suggests that an optimum distribution of small uniform micropores is achieved by maximising chain rigidity and internal free volume of the constituent monomer units. Molecular modelling confirms the high chain rigidity and shows that PIM-MP-TB has fewer interconnected pores than other common PIMs, which explains its relatively low permeability in combination with a strongly size sieving nature. Most importantly, gas permeability data of PIM-MP-TB approach those obtained from the triptycene-based PIMs KAUST-PI-1,[22] TPIM-1 [21] and PIM-Trip-TB,[24] which have been used to define the 2015 upper bounds for the H_2/CH_4, H_2/N_2 and O_2/N_2 gas pairs.[19] However, in contrast to these high performing PIMs, the synthesis of PIM-MP-TB is achieved in only four simple steps from a cheap starting material.

Conflicts of interest

There are no conflicts to declare.

Acknowledgements

The work leading to these results has received funding from the European Union's Seventh Framework Program (FP7/2007–2013) under grant agreement no. 608490, project M^4CO_2. Alessio Fuoco and Marcello Monteleone are gratefully acknowledged for their help in some of the gas permeation experiments.

Notes and references

1 P. M. Budd, B. S. Ghanem, S. Makhseed, N. B. McKeown, K. J. Msayib and C. E. Tattershall, *Chem. Commun.*, 2004, 230–231.
2 F. Xia, M. Pan, S. Mu, R. Malpass-Evans, M. Carta, N. B. McKeown, G. A. Attard, A. Brew, D. J. Morgan and F. Marken, *Electrochim. Acta*, 2014, **128**, 3–9.
3 X. Du, Y. Sun, B. Tan, Q. Teng, X. Yao, C. Su and W. Wang, *Chem. Commun.*, 2010, **46**, 970–972.

4 P. Kaur, J. T. Hupp and S. T. Nguyen, *ACS Catal.*, 2011, **1**, 819–835.
5 M. Carta, M. Croad, K. Bugler, K. J. Msayib and N. B. McKeown, *Polym. Chem.*, 2014, **5**, 5262–5266.
6 X. Weng, J. E. Baez, M. Khiterer, M. Y. Hoe, Z. Bao and K. J. Shea, *Angew. Chem., Int. Ed.*, 2015, **54**, 11214–11218.
7 Y. Wang, N. B. McKeown, K. J. Msayib, G. A. Turnbull and I. D. W. Samuel, *Sensors*, 2011, **11**, 2478–2487.
8 N. A. Rakow, M. S. Wendland, J. E. Trend, R. J. Poirier, D. M. Paolucci, S. P. Maki, C. S. Lyons and M. J. Swierczek, *Langmuir*, 2010, **26**, 3767–3770.
9 E. Madrid, Y. Rong, M. Carta, N. B. McKeown, R. Malpass-Evans, G. A. Attard, T. J. Clarke, S. H. Taylor, Y. T. Long and F. Marken, *Angew. Chem., Int. Ed.*, 2014, **53**, 10751–10754.
10 Y. Rong, A. Kolodziej, E. Madrid, M. Carta, R. Malpass-Evans, N. B. McKeown and F. Marken, *J. Electroanal. Chem.*, 2016, **779**, 241–249.
11 Z. Yang, R. Guo, R. Malpass-Evans, M. Carta, N. B. McKeown, M. D. Guiver, L. Wu and T. Xu, *Angew. Chem.*, 2016, **128**, 11671–11674.
12 M. Žák, M. Klepic, L. Č. Štastná, Z. Sedláková, H. Vychodilová, Š. Hovorka, K. Friess, A. Randová, L. Brožová and J. C. Jansen, *Sep. Purif. Technol.*, 2015, **151**, 108–114.
13 T. S. Anokhina, A. A. Yushkin, P. M. Budd and A. V. Volkov, *Sep. Purif. Technol.*, 2015, **156**, 683–690.
14 D. Fritsch, P. Merten, K. Heinrich, M. Lazar and M. Priske, *J. Membr. Sci.*, 2012, **401–402**, 222–231.
15 N. B. McKeown and P. M. Budd, *Macromolecules*, 2010, **43**, 5163–5176.
16 P. M. Budd and N. B. McKeown, *Polym. Chem.*, 2010, **1**, 63–68.
17 L. M. Robeson, *J. Membr. Sci.*, 1991, **62**, 165–185.
18 L. M. Robeson, *J. Membr. Sci.*, 2008, **320**, 390–400.
19 R. Swaidan, B. Ghanem and I. Pinnau, *ACS Macro Lett.*, 2015, **4**, 947–951.
20 L. M. Robeson, Q. Liu, B. D. Freeman and D. R. Paul, *J. Membr. Sci.*, 2015, **476**, 421–431.
21 B. S. Ghanem, R. Swaidan, X. Ma, E. Litwiller and I. Pinnau, *Adv. Mater.*, 2014, **26**, 6696–6700.
22 B. S. Ghanem, R. Swaidan, E. Litwiller and I. Pinnau, *Adv. Mater.*, 2014, **26**, 3688–3692.
23 M. Carta, R. Malpass-Evans, M. Croad, Y. Rogan, J. C. Jansen, P. Bernardo, F. Bazzarelli and N. B. McKeown, *Science*, 2013, **339**, 303–307.
24 M. Carta, M. Croad, R. Malpass-Evans, J. C. Jansen, P. Bernardo, G. Clarizia, K. Friess, M. Lanč and N. B. McKeown, *Adv. Mater.*, 2014, **26**, 3526–3531.
25 I. Rose, M. Carta, R. Malpass-Evans, M.-C. Ferrari, P. Bernardo, G. Clarizia, J. C. Jansen and N. B. McKeown, *ACS Macro Lett.*, 2015, **4**, 912–915.
26 I. Rose, C. G. Bezzu, M. Carta, B. Comesana-Gandara, E. Lasseuguette, M. C. Ferrari, P. Bernardo, G. Clarizia, A. Fuoco, J. C. Jansen, K. E. Hart, T. P. Liyana-Arachchi, C. M. Colina and N. B. McKeown, *Nat. Mater.*, 2017, **16**, 932–937.
27 H.-Y. Tsai, M.-H. Luo, T.-C. Fang, M.-J. Chang and K.-Y. Chen, *J. Chin. Chem. Soc.*, 2013, **60**, 166–170.
28 M. N. Paddon-Row and H. K. Patney, *Synthesis*, 1986, **1986**, 328–330.
29 K. Baathulaa, Y. Xu and X. Qian, *Nat. Protoc.*, 2011, **6**, 1990–1997.
30 F.-G. Klaerner, S. Madenci, M. C. Kuchenbrandt, D. Blaeser, R. Boese, G. Fukuhara and Y. Inoue, *Eur. J. Org. Chem.*, 2012, **2012**, 3385–3395.
31 Y. Shu, Y.-F. Lim, Z. Li, B. Purushothaman, R. Hallani, J. E. Kim, S. R. Parkin, G. G. Malliaras and J. E. Anthony, *Chem. Sci.*, 2011, **2**, 363–368.
32 R. G. Kostyanovsky, V. R. Kostyanovsky, G. n. K. Kadorkina and K. A. Lyssenko, *Mendeleev Commun.*, 2003, **13**, 111–113.
33 M. Carta, R. Malpass-Evans, M. Croad, Y. Rogan, M. Lee, I. Rose and N. B. McKeown, *Polym. Chem.*, 2014, **5**, 5267–5272.
34 M. Heuchel, D. Fritsch, P. M. Budd, N. B. McKeown and D. Hofmann, *J. Membr. Sci.*, 2008, **318**, 84–99.
35 E. Tocci, L. De Lorenzo, P. Bernardo, G. Clarizia, F. Bazzarelli, N. B. McKeown, M. Carta, R. Malpass-Evans, K. Friess, K. Pilnacek, M. Lanc, Y. P. Yampolskii, L. Straarannikova, V. Shantarovich, M. Mauri and J. C. Jansen, *Macromolecules*, 2014, **47**, 7900–7916.
36 W. Fang, L. Zhang and J. Jiang, *J. Phys. Chem. C*, 2011, **115**, 14123–14130.
37 P. M. Budd, N. B. McKeown, B. S. Ghanem, K. J. Msayib, D. Fritsch, L. Starannikova, N. Belov, O. Sanfirova, Y. Yampolskii and V. Shantarovich, *J. Membr. Sci.*, 2008, **325**, 851–860.
38 P. Bernardo, F. Bazzarelli, F. Tasselli, G. Clarizia, C. R. Mason, L. Maynard-Atem, P. M. Budd, M. Lanč, K. Pilnáček and O. Vopička, *Polymer*, 2017, **113**, 283–294.
39 D. Hofmann, M. Heuchel, Y. Yampolskii, V. Khotimskii and V. Shantarovich, *Macromolecules*, 2002, **35**, 2129–2140.
40 J. C. Jansen, M. Macchione, E. Tocci, L. De Lorenzo, Y. P. Yampolskii, O. Sanfirova, V. P. Shantarovich, M. Heuchel, D. Hofmann and E. Drioli, *Macromolecules*, 2009, **42**, 7589–7604.
41 K. Nagai, A. Higuchi and T. Nakagawa, *J. Polym. Sci., Part B: Polym. Phys.*, 1995, **33**, 289–298.
42 V. Teplyakov and P. Meares, *Gas Sep. Purif.*, 1990, **4**, 66–74.